Journal of Power Sources 195 (2010) 2241–2247

Contents lists available at ScienceDirect

Journal of Power Sources

journal homepage: www.elsevier.com/locate/jpowsour

# The effect of hydrogen crossover on open-circuit voltage in polymer electrolyte membrane fuel cells

Saurabh A. Vilekar, Ravindra Datta*

*Fuel Cell Center, Department of Chemical Engineering, Worcester Polytechnic Institute, Worcester, MA 01609, United States*

ARTICLE INFO

*Article history:*
Received 27 August 2009
Received in revised form 12 October 2009
Accepted 12 October 2009
Available online 21 October 2009

*Keywords:*
Open-circuit voltage (OCV)
Crossover current
Fuel permeation
Hydrogen crossover
Oxygen crossover
Short-circuiting current

ABSTRACT

Even though the measured open-circuit voltage in a $H_2$–$O_2$ PEM fuel cell is invariably about 200–250 mV lower than that predicted from thermodynamics (1.229 V at 25 °C), there is no unequivocal explanation of this phenomenon available in the literature, although several hypotheses exist. Based on a theoretical model of mixed potential with *a priori* parameters, it is shown here that this voltage loss under open-circuit conditions can be attributed exclusively to hydrogen crossover and the resulting oxygen reduction reaction overpotential at the cathode. The analytical model predictions agree well with available experimental results.



## 1. Introduction

It is an irksome fact of life that the open-circuit voltage (OCV) of the low temperature polymer electrolyte membrane (PEM) fuel cell is typically only around 0.95–1.05 V, as shown in Fig. 1 [1] versus temperature, rather than the reversible voltage $V_0$ (1.229 V at 25 °C) promised by thermodynamics. What is worse is that, despite extensive study over the course of three-quarters of a century, there is no clear explanation in the literature for this loss of around 20% in OCV, which causes a corresponding loss in the fuel cell efficiency, since efficiency of a fuel cell, $\varepsilon = (V/V_0)\varepsilon_0$, where $V$ is the fuel cell voltage, $V_0$ is the thermodynamic voltage, and $\varepsilon_0$ is the thermodynamic efficiency. Clearly, an unambiguous understanding of the main reason for this in PEM fuel cells is important, which is the objective of this paper.

The various hypotheses advanced to rationalize this observation center around the extremely low-exchange current density for the 4-electron oxygen reduction reaction (ORR) on Pt ($i_0^* \sim 10^{-10}$ A cm$^{-2}$) coupled with one or more side reactions occurring at the cathode in addition to the ORR [2,3]. The presence of side reactions results in either a "rest potential," i.e., an *equilibrium* potential for a closed system, or a "mixed potential," i.e., a *steady-state* potential for an open system, e.g., a fuel cell, that is significantly lower than the thermodynamic potential (Fig. 1). Some of the possible side reactions $\rho$ proposed are summarized in Table 1 [3], which can, of course, proceed in either direction depending upon the overpotential of electrode reaction $\rho$, $\eta_\rho = \Phi - \Phi_{\rho,0}$, where $\Phi$ is the electrode (rest, or mixed) potential, and $\Phi_{\rho,0}$ is the equilibrium potential for an individual reaction $\rho$. However, there is little consensus on which, if any, is the dominant parasitic reaction in this list.

If the fuel cell OCV were determined by the thermodynamic equilibrium potential in the presence of side reactions, the overpotential $\eta_\rho$ as well as the net current of each electrode reaction $\rho$ must individually be zero, i.e., $i_\rho = \vec{i}_\rho - \overleftarrow{i}_\rho = 0$, so that the rest potential $\Phi = \Phi_{\rho,0}$ is determined via simultaneous solution of the corresponding Nernst equations for the independent reaction set

$$\Phi_{\rho,0} = \Phi^o_{\rho,0} + \frac{RT}{\nu_{\rho e^-} F} \ln \prod_{\substack{i=1 \\ i \neq e^-}}^{n} a_i^{\nu_{\rho i}} \quad (1)$$

where $\Phi^o_{\rho,0}$ is the standard electrode potential, i.e., for unit activities $a_i$ of species $i$, and $\nu_{\rho i}$ is its stoichiometric coefficient in reaction $\rho$, while $\nu_{\rho e^-}$ is that for electrons in it. For instance, if $H_2O_2$ were considered a side product, even though minor, at the cathode, there are two independent overall reactions (ORs) at the cathode, namely, the ORR (reaction 3 in Table 1), along with one more OR involving $H_2O_2$, e.g., reaction 7 in Table 1.

*Abbreviations:* HOR, hydrogen oxidation reaction; MEA, membrane electrode assembly; OCV, open-circuit voltage; ORR, oxygen reduction reaction; PEM, polymer electrolyte membrane; RH, relative humidity.

* Corresponding author. Tel.: +1 508 831 6036.
*E-mail address:* rdatta@wpi.edu (R. Datta).

0378-7753/$ – see front matter © 2009 Elsevier B.V. All rights reserved.
doi:10.1016/j.jpowsour.2009.10.023

## Nomenclature

| | |
|---|---|
| $c_i$ | concentration of the gaseous species $i$ within the Nafion |
| $D_i$ | diffusion coefficient of gaseous species $i$ within Nafion |
| $E_{\mathrm{HOR},\Phi_0}$ | effective activation energy for *HOR* |
| $E_{\mathrm{ORR},\Phi_0}$ | effective activation energy for ORR |
| $F$ | Faraday's constant, 96,487 C eq$^{-1}$ |
| $i$ | fuel cell current density (A cm$^{-2}$ of geometric electrode area) |
| $i_{\mathrm{int}}$ | total internal current consisting of short-circuiting and crossover currents, A cm$^{-2}$ |
| $i_{S,M}$ | electrical-short-circuit current |
| $i_{X,C}$ | crossover current at the cathode |
| $i_{X,A}$ | crossover current at the anode |
| $i_0$ | exchange current density (A cm$^{-2}$ of geometric electrode area) |
| $i^*$ | current density (A cm$^{-2}$ of metal catalyst surface) |
| $i_0^*$ | exchange current density (A cm$^{-2}$ of metal catalyst surface) |
| $i_{0,ref}^*$ | exchange current density at reference conditions (A cm$^{-2}$ of metal catalyst surface) |
| $i_{A,L}$ | anode limiting current density (A cm$^{-2}$) |
| $i_{C,L}$ | cathode limiting current density (A cm$^{-2}$) |
| $k_i$ | permeability of gaseous species $i$ within Nafion |
| $\kappa_i$ | partition coefficient of gaseous species $i$ within Nafion |
| $k_{\mathrm{H_2}}$ | permeability of hydrogen within Nafion |
| $k_{\mathrm{O_2}}$ | permeability of oxygen within Nafion |
| $L_M$ | membrane thickness |
| $L_{\mathrm{EL}}$ | thickness of the electrolyte ($L_{EL} = L_M$) |
| $N_{i,z}$ | flux of species $i$ in the membrane along the $z$ direction |
| OCV | open-circuit voltage (V) |
| $p_i$ | partial pressure of species $i$ (atm) |
| $R$ | gas constant (J mol$^{-1}$ K$^{-1}$) |
| $R_I$ | Interfacial resistance ($\Omega$ cm$^2$) |
| $T$ | Temperature (K) |
| $T_{ref}$ | Reference temperature (K) |
| $V_0$ | Thermodynamic open-circuit potential = $(\Phi_{0,C} - \Phi_{0,A})$ (V) |
| $V$ | Fuel cell voltage (V) |

*Greek symbols*

| | |
|---|---|
| $\varepsilon$ | fuel cell efficiency |
| $\Phi$ | electrode potential |
| $\Phi_{\rho,0}$ | half-cell thermodynamic (reversible) potential (V) of electrode reaction $\rho$ |
| $\Phi^o_{\rho,0}$ | standard half-cell thermodynamic potential (V) of electrode reaction $\rho$, i.e., for unit activities |
| $\Phi_C$ | cathode potential |
| $\Phi_{A,0}$ | thermodynamic potential of HOR |
| $\eta_\rho$ | overpotential of electrode reaction $\rho = \Phi - \Phi_{\rho,0}$(V) (V) |
| $\eta_{X,A}$ | anodic overpotential (V) |
| $\eta_{X,C}$ | cathodic overpotential (V) |
| $\nu_{\rho i}$ | stoichiometric coefficient of species $i$ in reaction $\rho$ |
| $\nu_{\rho \mathrm{e}^-}$ | stoichiometric coefficient of electrons in reaction $\rho$ |
| $\alpha_\rho^\bullet$ | effective transfer coefficient of the electrode reaction $\rho$ |
| $\gamma_M$ | roughness factor (cm$^2$ metal cm$^{-2}$ geometric electrode area) |
| $\sigma_{M,\mathrm{e}^-}$ | electronic conductivity of the membrane |
| $\sigma_{EL}$ | protonic conductivity of the membrane |

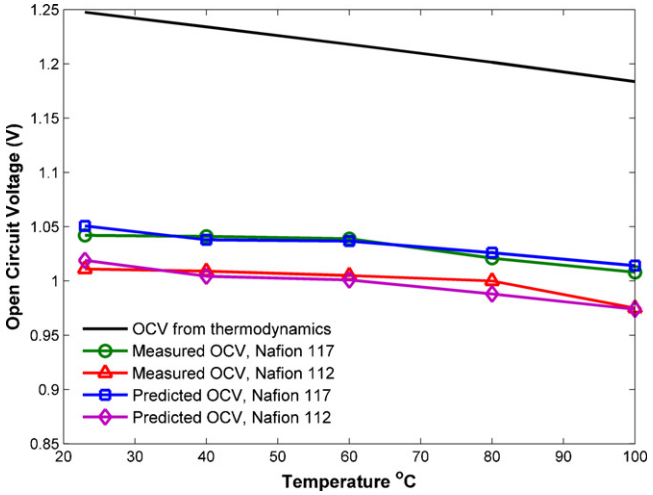


**Fig. 1.** Model prediction of open-circuit voltage (OCV) for a PEM fuel cell as a function of temperature and membrane thickness. Experimental values are taken from Ref. [1] (anode: $H_2$, cathode: air, 3 atm, 100% RH).

On the other hand, in a steady-state system, the overpotentials $\eta_\rho \neq 0$, and are such that the currents from anodic (electron generating) and cathodic (electron consuming) reactions occurring simultaneously on the electrode add up to zero, i.e., there is no net current, $\sum_\rho i_\rho = 0$, which determines the resulting mixed potential $\Phi$ as well as the parasitic current, as shown schematically in Fig. 2. In other words, there is at least one anodic reaction occurring at the cathode that provides the electrons and protons consumed by the cathodic ORR and resulting in an overpotential. This, of course, is akin to corrosion.

Thus, a common explanation for the OCV is the formation of $H_2O_2$ via one of the reactions mentioned in Table 1, which could, in principle, alter the cathode thermodynamic potential. Alternately, the presence of $H_2O_2$ could sustain an anodic current density necessary for a mixed potential. However, it has been argued that the concentration of any $H_2O_2$ is far too small for this [3].

An alternate explanation involves the presence of surface oxides via Pt corrosion via one or more reactions mentioned in Table 1. However, in an open system such as a fuel cell, reactions involving Pt or C support (reaction 8 in Table 1) cannot go on indefinitely and, hence, must also be rejected as the explanation for the observed OCV.

The explanation favored by Bockris and Srinivasan [3] in the study of the half-cell open-circuit potential of ORR in a liquid electrolyte, is an anodic oxidation reaction (reaction 9 in Table 1) due to

**Table 1**
Possible reactions involving $O_2$, $H_2$, carbon support C, impurity $CH_x$, and Pt at the PEM fuel cell cathode [3].

| Reaction no., $\rho$ | Overall reaction | Standard electrode potential, $\Phi^o_{\rho,0}$ (V) |
|---|---|---|
| 1 | $H_2O_2 + 2H^+ + 2e^- \leftrightarrows 2H_2O$ | 1.77 |
| 2 | $PtO_3 + 2H^+ + 2e^- \leftrightarrows PtO_2 + H_2O$ | 1.48 |
| 3 | $O_2 + 4H^+ + 4e^- \leftrightarrows 2H_2O$ | 1.229 |
| 4 | $PtO_2 + 2H^+ + 2e^- \leftrightarrows Pt(OH)_2$ | 1.11 |
| 5 | $Pt(OH)_2 + 2H^+ + 2e^- \leftrightarrows Pt + 2H_2O$ | 0.98 |
| 6 | $PtO + 2H^+ + 2e^- \leftrightarrows Pt + H_2O$ | 0.88 |
| 7 | $O_2 + 2H^+ + 2e^- \leftrightarrows H_2O_2$ | 0.68 |
| 8 | $C + 2H_2O \leftrightarrows CO_2 + 4H^+ + 4e^-$ | 0.207 |
| 9 | $CH_x + 2H_2O \leftrightarrows CO_2 + (x+4)H^+ + (x+4)e^-$ | ? |
| 10 | $2H^+ + 2e^- \leftrightarrows H_2$ | 0.00 |

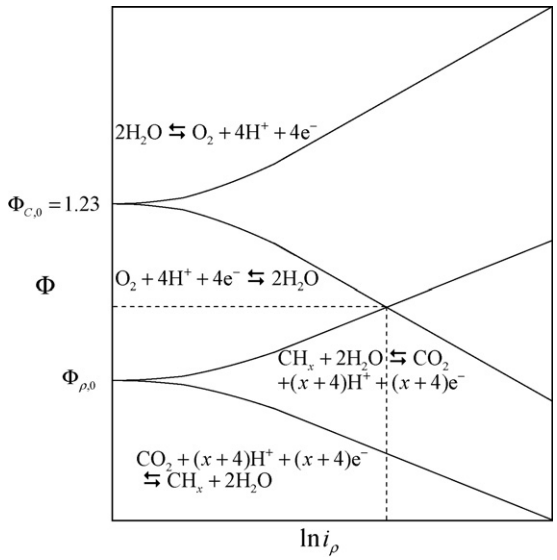


**Fig. 2.** Current–potential curves for ORR and a hypothetical impurity oxidation reaction intersecting at mixed potential and a corresponding parasitic current.

the presence of "an organic impurity present at low concentrations in solution and having a reversible potential of 0.2–0.3 V" that compromises the cathodic current of the ORR, i.e., reaction 3 in Table 1. In careful experiments they found that the OCV tended toward the 1.23 V value for the ORR when care was taken to rigorously free the electrolyte solution of any traces of impurities. A schematic representation of the resulting mixed potential is given in Fig. 2, showing anodic and cathodic potential versus current relations for ORR and the oxidation of an organic impurity, the intersection of the two curves representing the graphical solution for OCV as the mixed potential. However, again this explanation involving an organic impurity seems unlikely for the OCV of a $H_2$–$O_2$ PEM fuel cell operating for hundreds or thousands of hours.

A more plausible explanation attributes the observed OCV in an operating fuel cell to $H_2$ crossover and/or internal electrical short-circuiting [4]. Thus, Laraminie and Dicks [4] suggest that the electrolyte supports a very small amount of electronic conductivity, so that small short-circuiting currents are possible. More importantly, however, they propose that hydrogen crossover supports a small "internal current" of around, $i_X \approx 2$ mA, which can cause an activation overpotential of around 0.3 V at the cathode, estimated based on a Tafel equation, $\eta = b \ln(i_X/i_0)$, for ORR with empirical parameters, i.e., a Tafel slope $b = 60$ mV, and an ORR-exchange current density $i_0$=4.0 × $10^{-5}$ mA $cm^{-2}$. Our more careful theoretical analysis below based on *a priori* parameters supports the latter explanation as the exclusive reason for the observed phenomenon.

A more recent experimental investigation of Zhang et al. [1] on the effect of temperature on OCV considered a variety of possible explanations: (1) reduced partial pressures of $O_2$ and $H_2$ at higher temperatures due to humidification, as explained by the Nernst equation, (2) mixed potential of the Pt/PtO catalyst surface, and (3) hydrogen crossover. They concluded that the loss of OCV is due mainly (135 mV at 80 °C) to the Pt/PtO catalyst surface, and secondarily (56 mV at 80 °C with Nafion 112) to hydrogen crossover.

In another recent study on membrane degradation and OCV, Sompalli et al. [5] also assume that the OCV is determined by the parasitic current caused by a combination of the permeation of $H_2$ and Ohmic shorting through the membrane, the latter being a minor contributor. Like Laraminie and Dicks [4], these authors calculate the resulting cathode overpotential via an empirical Tafel equation. Further, they propose OCV as a key diagnostic indicator of membrane health [5]. Thus, membrane thinning and pinhole formation leads to an increase in hydrogen crossover and consequently a decline in OCV. They further reason that the OCV is higher at lower relative humidity (RH), due to the lower $H_2$ crossover rate [5]. Based on the hypothesis that higher OCVs lead to enhanced chemical degradation of the membrane, the degradation rate would thus be higher at lower RH. They further conclude that any parasitic currents caused by carbon corrosion at the cathode are also negligible, being an order of magnitude smaller as compared with those from hydrogen crossover (0.1–1 mA $cm^{-2}$).

In short, despite its ubiquitous nature and practical significance, there is an absence of a clear, quantitative, and unambiguous explanation for the observed OCV in a low temperature PEM fuel cell. We theoretically analyze below the role of hydrogen crossover in PEM fuel cells, in shortchanging the OCV from its promised value of around 1.23 V, and show that hydrogen crossover can, in fact, explain the entire potential loss under open-circuit conditions. Further, it is able to rationalize the commonly observed effect of temperature and the presence of any pinholes or membrane thinning on the drop in OCV of a PEM fuel cell.

## 2. Theory

A schematic of the various processes that occur as a result of the permeation is provided in Fig. 3. Thus, as shown in Fig. 3, even though there is no external current $i$ under open-circuit conditions, there are internal short-circuiting currents $i_{int}$ because of: (1) the minor electronic conductivity of the electrolyte membrane, namely the electrical-short-circuit current, $i_{S,M}$; and (2) due to the permeating $H_2$ and $O_2$ across the membrane that cause small local crossover currents at the cathode and the anode, respectively (i.e., $i_{X,C}$ and $i_{X,A}$), thus polarizing the two electrodes even under open-circuit conditions.

The $H_2$ that permeates over to the cathode from the anode can, in principle, undergo oxidation on the Pt catalyst with $O_2$ either chemically, or electrochemically, or via both of these pathways. However, keeping in mind that the cathode potential $\Phi_C$ is very high (~1.0 V) as compared to the thermodynamic potential of hydrogen oxidation reaction (HOR), i.e., $\Phi_{A,0} = 0.0$ V, there is a huge overpotential of around $\eta \sim 1.0$ V for the HOR at the cathode, thus dramatically enhancing the electrochemical route, and making it the likely pathway [6]. Therefore, we will ignore the chemical route to the hydrogen oxidation at the cathode. Thus, the electrochemical HOR provides electrons, or a crossover current at cathode, $i_{X,C}$, for the ORR at the cathode even under open-circuit conditions (Fig. 3).

Similarly, in principle, there is some ORR occurring at the anode because of the small amount of $O_2$ permeating through the PEM

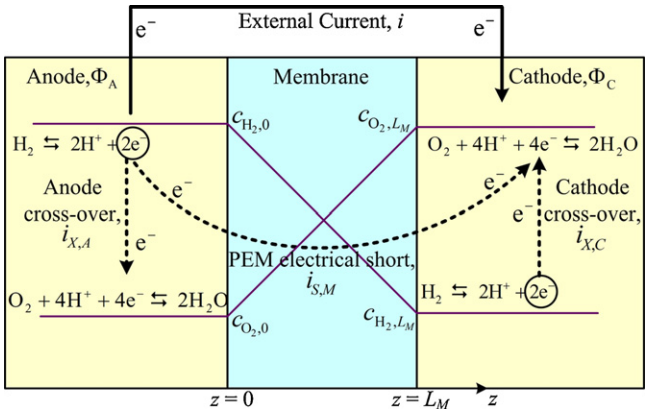


**Fig. 3.** Schematic representation of various electrode reactions and the resulting external and internal crossover and electrical short-circuit currents.

from the cathode to the anode. This robs electrons from the HOR occurring at the anode, thus resulting in a crossover current at anode, $i_{X,A}$ (Fig. 3). In addition, there is an electrical-short-circuit current across the PEM, $i_{S,M}$ even under open-circuit conditions due to the tiny electronic conductivity of the electrolyte, as shown schematically in Fig. 3. Thus, the total internal current, $i_{\text{int}}$ at a given electrode consists of the electrical-short-circuit current and the crossover current due to fuel permeation, e.g., at the cathode, $i_{\text{int},C} = i_{X,C} + i_{S,M}$.

In other words, the open-circuit condition is not strictly an equilibrium condition, but is rather a steady-state condition with small internal currents. As mentioned above, the steady-state condition is defined at each electrode by the sum over all electrode reactions (HOR and ORR) at a given electrode, $\sum_{\rho} i_\rho = 0$, rather than by individual $i_\rho = 0$, as required by the equilibrium condition. Thus, at either electrode, the current for the HOR and that for the ORR are equal and opposite at steady state, akin to corrosion currents.

These parasitic currents cause overpotentials at the anode and the cathode, so that the observed OCV is given as

$$\text{OCV} = V_0 - \eta_{X,A} + \eta_{X,C} \tag{2}$$

where $\eta_\rho = \Phi - \Phi_{\rho,0}$ is the overpotential for the electrode reaction $\rho$. Thus, it is positive for anode and negative for the cathode.The thermodynamic cell voltage, $V_0 = (\Phi_{0,C} - \Phi_{0,A})$. For the case of liquid water being produced in the low temperature PEM fuel cell, i.e., for $2H_2 + O_2 \leftrightarrows 2H_2O(l)$, the thermodynamic voltage is

$$V_0 = 1.229 - 8.46 \times 10^{-4}(T - 298) + \frac{RT}{4F} \ln p_{H_2}^2 p_{O_2} \tag{3}$$

In order to compute the crossover electrode overpotentials $\eta_{X,A}$ and $\eta_{X,C}$ under open-circuit conditions, let us first consider the crossover flux of gaseous species $i$ ($H_2$ or $O_2$) across the PEM. Under steady state, isothermal conditions, and no reaction within the Nafion layer, the one-dimensional species diffusion equation in Cartesian coordinates may be integrated subject to (Fig. 3):

$$\left.\begin{array}{ll} \text{B.C. 1}: & \text{at } z = 0, \quad c_i\big|_{z=0} = c_{i,0} \\ \text{B.C. 2}: & \text{at } z = L_M, \quad c_i\big|_{z=L_M} = c_{i,L_M} \end{array}\right\} \tag{4}$$

to provide the concentration profile of species $i$ within the electrolyte layer

$$\frac{c_{i,0} - c_i}{c_{i,0} - c_{i,L_M}} = \frac{z}{L_M} \tag{5}$$

i.e., the concentration profile within the membrane is linear for both $H_2$ and $O_2$ (Fig. 3).

The species flux in the membrane then from Fick's law is

$$N_{i,z} = \frac{D_i}{L_M}(c_{i,0} - c_{i,L_M}) = \frac{k_i}{L_M}(p_{i,0} - p_{i,L_M}) \tag{6}$$

where $c_i$ is the concentration of the gaseous species $i$ within the Nafion phase, $D_i$ is the diffusion coefficient of $i$ within Nafion, and the membrane permeability, $k_i = D_i\kappa_i/RT$ (mol atm$^{-1}$ s$^{-1}$). Here, the partition-coefficient, $\kappa_i = (c_i/c_{iG})_{eq}$ represents the solubility of the gaseous species $i$ in the membrane.

The permeating species ($H_2$ or $O_2$) undergoes electrochemical reaction $\rho$ (HOR or ORR) at the electrode, as shown schematically in Fig. 3. Thus, the corresponding current density

$$i_X = F\nu_{\rho e^-} N_{i,z} \tag{7}$$

where $F$ is the Faraday's constant. At steady-state, this diffusion flux is equal to the rate of the electrode reaction, which may be described via Butler–Volmer equation of the form [7]

$$i_X = i_0 \left\{ 2\sinh\left( \frac{\alpha_\rho^\bullet \nu_{\rho e^-}^\bullet F\eta_\rho}{RT} \right) \right\} \tag{8}$$

where $\alpha_\rho^\bullet$ is the effective transfer coefficient of the electrode reaction $\rho$, taken as symmetry factor of the rate-limiting step (RLS) (typically 1/2) in the sequence of molecular steps involved in the electrode reaction $\rho$, and $\nu_{\rho e^-}^\bullet$ is the stoichiometric coefficient of electrons in the RLS.

In the above, the exchange current density on the basis of the geometric electrode area [7]

$$i_X = \gamma_M i_X^*; i_0 = \gamma_M i_0^* \tag{9}$$

where $\gamma_M$ is the catalyst roughness factor, and the current density with the asterisk, $i_0^*$, is defined in terms of per unit active metal catalyst surface area. Further, the exchange-current density under actual conditions in a PEM fuel cell is related to that under reference conditions via

$$i_0 = \gamma_M \left( \frac{p_i}{p_{i,ref}} \right) \exp\left\{ -\frac{E_{\Phi_0}}{R} \left( \frac{1}{T} - \frac{1}{T_{ref}} \right) \right\} i_{0,ref}^* \tag{10}$$

where $p_i$ is the partial pressure of the permeating species at the electrode.

The final equation needed for the steady-state at an electrode under OCV conditions (i.e., when the external current $i = 0$) is

$$\sum_{\rho} i_\rho = 0 \tag{11}$$

i.e., the sum of current densities of HOR and ORR occurring at an electrode (anode or cathode) is zero. Finally, for completeness, we must account for the electrical-short-circuit current $i_{S,M}$ across the PEM as well, which from Ohm's law

$$i_{S,M} \approx V \left( \frac{\sigma_{M,e^-}}{L_M} \right) \tag{12}$$

where $\sigma_{M,e^-}$ is the electronic conductivity of the membrane. This current must be added to the crossover currents at the two electrodes to compute the overpotential.

## 3. PEM fuel cell analysis

Let us apply the above analysis to the crossover of $H_2$ and the ensuing HOR at the cathode (Fig. 3). The crossover current density corresponding to the hydrogen flux in the membrane is

$$i_{X,C} = \frac{(F\nu_{HOR,e^-})k_{H_2}}{L_M}(p_{H_2,0} - p_{H_2,L_M}) \tag{13}$$

which is also equal to that from the HOR kinetics at the cathode at the overpotential $\eta_{X,C}$

$$i_{X,C} = \gamma_{M,C} i_{HOR,0,ref}^* \left( \frac{p_{H_2,L_M}}{p_{H_2,ref}} \right) \exp\left\{ -\frac{E_{HOR,\Phi_0}}{R} \left( \frac{1}{T} - \frac{1}{T_{ref}} \right) \right\} \times 2\sinh\left\{ \frac{\alpha_{HOR}^\bullet \nu_{HOR,e^-}^\bullet F(\eta_{X,C} + V_0)}{RT} \right\} \tag{14}$$

where we have combined the Butler–Volmer equation with the correlation for exchange-current density. Of course, since this is equal and opposite of the ORR current at the cathode

$$i_{X,C} = \gamma_{M,C} i_{ORR,0,ref}^* \left( \frac{p_{O_2,L_M}}{p_{O_2,ref}} \right) \exp\left\{ -\frac{E_{ORR,\Phi_0}}{R} \left( \frac{1}{T} - \frac{1}{T_{ref}} \right) \right\} \times 2\sinh\left\{ \frac{\alpha_{ORR}^\bullet \nu_{ORR,e^-}^\bullet F(\eta_{X,C})}{RT} \right\} \tag{15}$$

The above 3 equations, Eqs. (13)–(15) contain 3 unknowns, namely, the partial pressure of $H_2$ at the cathode $p_{H_2,L_M}$, the crossover current at the cathode $i_{X,C}$, and the cathode overpotential $\eta_{X,C}$ under open-circuit conditions, which can all hence be found via simultaneous solution.

## 4. Limiting case

Let us consider the limiting case when $p_{H_2,L_M} \to 0$. This is entirely plausible because of the very high overpotential at the cathode for HOR. Then the solution is greatly simplified. Thus, from Eq. (13), we have

$$i_{X,C} \approx \frac{(F\nu_{HOR,e^-})k_{H_2}}{L_M} p_{H_2,0} \tag{16}$$

which can, hence, be directly evaluated from the permeability data for $H_2$. Thereupon, the cathode overpotential $\eta_{X,C}$ can be found from either of the two kinetics equations for HOR or ORR above (Eq. (14) or (15)). Finally, including the electrical-short-circuit current $i_{S,M}$, Eq. (12), as well, we have

$$\eta_{X,C} = \left(\frac{RT}{\alpha^{\bullet}_{ORR}\nu^{\bullet}_{ORR,e^-}F}\right) \sinh^{-1}\left\{\frac{(F\nu_{HOR,e^-})k_{H_2}p_{H_2,0} + V\sigma_{M,e^-}}{2L_M i_{ORR,0}}\right\} \tag{17}$$

An identical analysis can be done for the permeation of $O_2$, and the resulting open-circuit anode overpotential. For the limiting case, as above,

$$\eta_{X,A} = \left(\frac{RT}{\alpha^{\bullet}_{HOR}\nu^{\bullet}_{HOR,e^-}F}\right) \sinh^{-1}\left\{\frac{(F\nu_{ORR,e^-})k_{O_2}p_{O_2,L_M} + V\sigma_{M,e^-}}{2L_M i_{HOR,0}}\right\} \tag{18}$$

Eqs. (17) and (18) may finally be substituted into Eq. (2) to evaluate $V$, i.e., OCV. In the event that the electronic conductivity of the membrane is small, the second term in the curly brackets can further be neglected. Clearly, however, the validity of the model depends upon the veracity of the model parameters, discussed next.

## 5. Model parameters

Sakai et al. [8,9] hypothesized that $H_2$ or $O_2$ permeates mainly through the hydrated ion-cluster regions of the Nafion membrane, while Broka and Ekdunge [10] suggest that the permeation process involves both, the hydrated ionic clusters and the amorphous region of Nafion. It is known, thus, that hydrated Nafion has higher gas permeability as compared to dry Nafion but lower than that in water [6]. Thus, dry Nafion has permeability coefficient for $H_2$ or $O_2$ similar to or lower than that for Teflon, while hydrated Nafion membrane has permeability coefficient approaching that in water [6,8,9]. We use the correlation provided by Kocha et al. [6] for the permeability of hydrogen in Nafion

$$k_{H_2} = 6.6 \times 10^{-8} \exp\left(-\frac{21,030\,\mathrm{J\,mol^{-1}}}{RT}\right) \mathrm{mol\,bar^{-1}\,cm^{-1}\,s^{-1}} \tag{19}$$

The permeability of oxygen in Nafion is approximately half that of hydrogen in Nafion [6,8,10]. Thus, we assume

$$k_{O_2} = \frac{k_{H_2}}{2} \mathrm{mol\,bar^{-1}\,cm^{-1}\,s^{-1}} \tag{20}$$

The electrical conductivity of Nafion, however, is not as well documented in the literature. Using a similar rationale as above, the electrical resistivity of Nafion in the dry state may be expected to be close to that of Teflon, while in the hydrated state it would be approaching the electrical resistivity of deionized water. The resistivity of Nafion at 50% RH is about $6\times10^5\,\Omega\,\mathrm{cm}$ [11], which provides an estimate for the electrical conductivity of Nafion, $\sigma_{M,e^-} \approx 1 \times 10^{-6}\,\mathrm{S\,cm^{-1}}$, a value similar to the electrical conductivity of water in equilibrium with $CO_2$ in air [12]. On the other hand, Sompalli et al. [5] give a membrane electronic resistance of $1–20\,\mathrm{k\Omega\,cm^2}$, which results in $0.1–0.02\,\mathrm{mA\,cm^{-2}}$.

**Table 2**
Roughness factor ($\mathrm{cm^2}$ metal $\mathrm{cm^{-2}}$ geometric electrode area) for anode and cathode as determined by Song et al. [13] in low current density region, measured at 3.0 atm pressure and 100% RH.

| Temperature (°C) | $\gamma_{M,\mathrm{Anode}}$ | $\gamma_{M,\mathrm{Cathode}}$ |
|---|---|---|
| 23 | 44.5 | 305.0 |
| 40 | 28.3 | 168.0 |
| 60 | 28.3 | 152.0 |
| 80 | 30.7 | 106.0 |
| 100 | 13.0 | 78.0 |

For the HOR, we further assume $\alpha^{\bullet}_{HOR} = 1/2$, and the exchange-current density $i^{*}_{HOR,0,ref} = 1 \times 10^{-3}\,\mathrm{A\,cm^{-2}}$ of metal catalyst surface, commonly reported in the literature [7]. The effective activation energy for HOR on PtRu/C is taken as $E_{HOR,\Phi_0} = 34.6\,\mathrm{kJ\,mol^{-1}}$, higher than that on Pt [13]. For the ORR the exchange-current density is of the order $10^{-10}\,\mathrm{A\,cm^{-2}}$, i.e., $i^{*}_{ORR,0,ref} = 1 \times 10^{-10}\,\mathrm{A\,cm^{-2}}$ of metal catalyst surface [14]. We use $\alpha^{\bullet}_{ORR} = 1/2$, and the effective activation energy on Pt/C as given by Neyerlin et al. [15], is taken as $E_{ORR,\Phi_0} = 67\,\mathrm{kJ\,mol^{-1}}$.

The roughness factor may be estimated using catalyst loading and nanoparticles size [7]. However, here we simply adopt the values reported by Song et al. [13], obtained experimentally utilizing the surface cyclic voltammetry measurements as shown in Table 2. Thus, all the model parameters are adopted from the literature as discussed above, and are summarized in Table 3.

## 6. Results and discussion

Zhang et al. [1] have experimentally monitored the OCV for PEM fuel cell with $H_2$ as the anode feed and air as the cathode. In their experiments, the anode and cathode consisted of PtRu/C and Pt/C, respectively with a total loading of $1.0\,\mathrm{mg\,cm^{-2}}$, and the roughness factors for the anode and the cathode provided in Table 2. Thus, Eqs. (2), (17) and (18) are solved simultaneously to calculate the OCV using the parameters from Table 2 and Table 3. Fig. 1 compares the model predictions with experimental observations of Zhang et al. [1] for PEM fuel cell at 100% RH and 3.0 atm pressure, as a function of temperature and membrane thickness. The comparison between theory and experiments is hence quantitative with no fitted parameters. Further, as expected, the thicker membrane (Nafion 117) would have lower crossover currents and hence, higher observed OCV. Finally, the variation in the observed OCV as a function of temperature depends on a number of parameters, e.g., ORR activation energy, roughness factor. In this particular

**Table 3**
Parameters employed in the OCV model.

| Parameter | Value | Units |
|---|---|---|
| $k_{H_2}$ | $6.6 \times 10^{-8} \exp\left(-\frac{21030\,\mathrm{J\,mol^{-1}}}{RT}\right)$ | $\mathrm{mol\,bar^{-1}\,cm^{-1}\,s^{-1}}$ |
| $k_{O_2}$ | $\frac{k_{H_2}}{2}$ | $\mathrm{mol\,bar^{-1}\,cm^{-1}\,s^{-1}}$ |
| $\sigma_{M,e^-}$ | $1 \times 10^{-6}$ | $\mathrm{S\,cm^{-1}}$ |
| $\alpha^{\bullet}_{HOR}$ | 1/2 | – |
| $i^{*}_{HOR,0,ref}$ | $1 \times 10^{-3}$ | $\mathrm{A\,cm^{-2}}$ |
| $E_{HOR,\Phi_0}$ # | 34.6 | $\mathrm{kJ\,mol^{-1}}$ |
| $\alpha^{\bullet}_{ORR}$ | 1/2 | – |
| $i^{*}_{ORR,0,ref}$ * | $1 \times 10^{-10}$ | $\mathrm{A\,cm^{-2}}$ |
| $E_{ORR,\Phi_0}$ | 67.0 | $\mathrm{kJ\,mol^{-1}}$ |
| $T_{ref}$ | 293 | K |
| $c_{H_2,ref}$ | $3.96 \times 10^{-5}$ | $\mathrm{mol\,cm^{-3}}$ |
| $c_{O_2,ref}$ | $8.32 \times 10^{-6}$ | $\mathrm{mol\,cm^{-3}}$ |

* Activation energy for Pt/C.
\# Activation energy for PtRu/C.

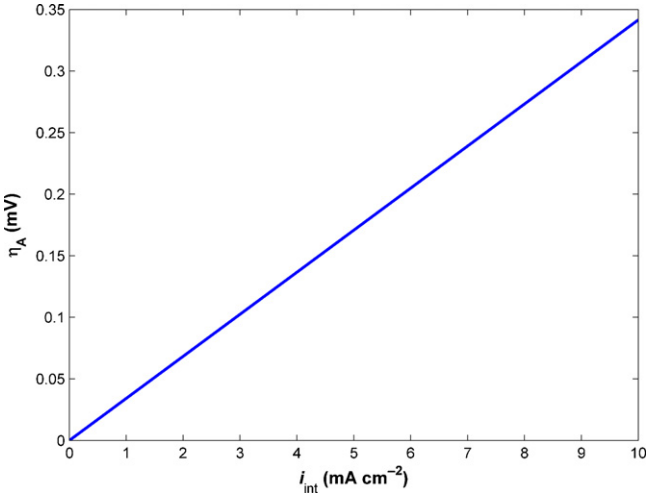


**Fig. 4.** Anode overpotential as a function of total internal current.

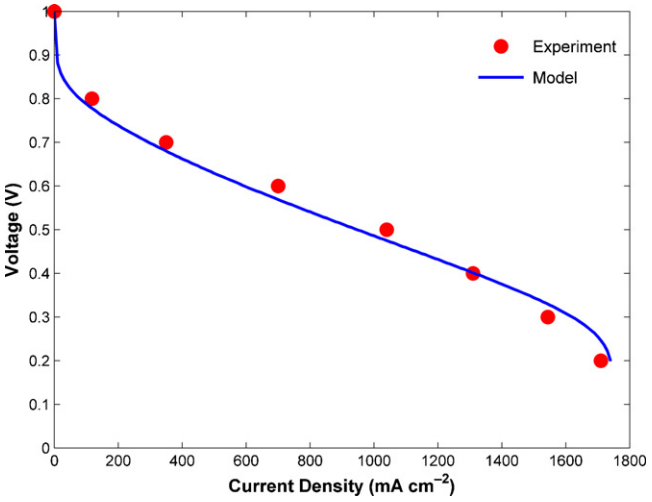


**Fig. 6.** Polarization curve for $H_2$–$O_2$ fuel cell with Pt/C electrodes (0.5 mg cm$^{-2}$) from ETEK, Nafion 115, $T = 70\,^{\circ}$C, $P = 1$ atm, 100% RH, $\sigma_{EL} = 0.1$ S cm$^{-1}$, $E_{A,\Phi_0} = 18$ kJ mol$^{-1}$ for Pt/C, $i_{C,L} = 1.75$ A cm$^{-2}$, $i_{A,L} = 4$ A cm$^{-2}$, $R_l = 0$, $\gamma_M = 116.62$. Rest of the values are provided in Table 3.

case, the change in slope of observed OCV may be attributable to the change in slope of the roughness factor as a function of temperature (Table 2).

In order to further investigate the relative significance of the hydrogen and oxygen crossover, Figs. 4 and 5 provide the effect of the total internal current, $i_{int}$ on the anode and cathode overpotential, respectively. It is evident from Fig. 4, that the anode overpotential is insignificant even for an internal current as high as 10 mA cm$^{-2}$. However, Fig. 5 indicates that the cathode overpotential is substantial and, in fact accounts for practically all of the observed incongruity between experimental OCV and the reversible potential. Further, we find that the electrical short-circuit current is approximately one order of magnitude lower than the crossover current for a pin-hole free MEA, an observation similar to that by Cleghorn et al. [16]. Thus, the Ohmic shorting does not noticeably affect the observed OCV. In view of this, thus, Eq. (17), can be further simplified into

$$\eta_{X,C} = \left(\frac{RT}{\alpha^{\bullet}_{ORR}\nu^{\bullet}_{ORR,e^-}F}\right)\sinh^{-1}\left\{\frac{(F\nu_{HOR,e^-})k_{H_2}p_{H_2,0}}{2L_M i_{ORR,0}}\right\} \quad (21)$$

Further, since the anode overpotential is negligible as compared to the cathode overpotential, we have, $V \approx V_0 + \eta_{X,C}$. Substituting

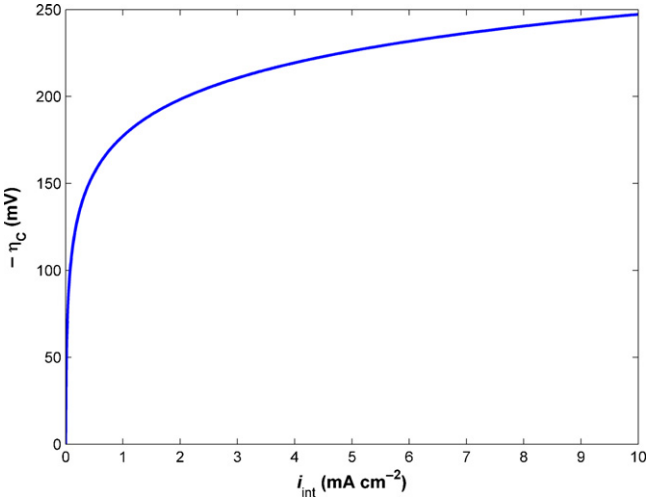


**Fig. 5.** Cathode overpotential as a function of total internal current.

Eqs. (3) and (21) in this, thus

$$\mathrm{OCV} = 1.229 - 8.46\times10^{-4}(T-298) + \frac{RT}{4F}\ln p^2_{H_2}p_{O_2} + \left(\frac{RT}{\alpha^{\bullet}_{ORR}\nu^{\bullet}_{ORR,e^-}F}\right)\sinh^{-1}\left\{\frac{(F\nu_{HOR,e^-})k_{H_2}p_{H_2,0}}{2L_M i_{ORR,0}}\right\} \quad (22)$$

In short, thus, the observed OCV at a given temperature and gas partial pressures and its deviation from the thermodynamic potential of 1.23 V is entirely explained by the cathode overpotential due to hydrogen permeation, which is adequately described by the above relation.

Additionally, in the presence of an external current $i$, the total current for the cathode is the sum of the external and the internal short-circuiting current. Then the corresponding $V$–$i$ relationship can be written as [7]

$$V = V_0 - \frac{RT}{\alpha^{\bullet}_{A}\nu^{\bullet}_{Ae^-}F}\sinh^{-1}\left\{\frac{1}{2}\left(\frac{i/i_{A,0}}{1-i/i_{A,L}}\right)\right\} + \frac{RT}{\alpha^{\bullet}_{C}\nu^{\bullet}_{Ce^-}F}\sinh^{-1}\left\{\frac{1}{2}\left(\frac{(i+i_{X,C})/i_{C,0}}{1-(i+i_{X,C})/i_{C,L}}\right)\right\} - i\left(\frac{L_{EL}}{\sigma_{EL}}\right) - i(R_l) \quad (23)$$

where the crossover current $i_{X,C}$ is given explicitly by Eq. (16). An example of a resulting plot is provided in Fig. 6. $\gamma_M = 116.62$ is predicted for the ETEK electrodes using correlations provided in Ref. [7]. It is evident that the predictions are reasonable with the *a priori* parameters, and that the crossover current makes a material difference only at very low current densities.

Pronounced effect of oxygen and hydrogen crossover on membrane degradation under open-circuit conditions have been reported by Inaba et al. [17] and Endoh et al. [18], respectively. Ionomer loss and membrane thinning has been observed under open-circuit conditions by Liu and Crum [19], which may result in pinhole formation and increased gas crossover. Of course, with the onset of membrane thinning and pinhole formation due to chemical degradation and fatigue, the crossover current increases, eventually leading to the failure of the MEA. It must be noted that gas crossover in the absence of catalyst does not cause membrane degradation. Consequently, the permeation of reactants and their subsequent

catalyzed electrochemical reaction is critical for the degradation of membrane. While the mechanism is not entirely clear, the high rate of membrane degradation at OCV may be attributed to $H_2O_2$ [20]. Thus, it may be argued that at the low cathode overpotential under OCV conditions, more $H_2O_2$ is produced, which is an intermediate species in the ORR. At higher overpotentials at the cathode, $H_2O_2$ can be further reduced into water. These qualitative observations insinuate a strong dependence between fuel permeation and OCV. Understanding the correlation between gas crossover and OCV, is thus of fundamental significance. The model presented in this study quantitatively shows that OCV is an indication of the fuel crossover and its electrochemical consumption, implicated by the enhanced membrane degradation under OCV conditions.

Furthermore, crossover of the reactant gases can also cause carbon corrosion [21]. Catalyst dissolution and precipitation within the membrane has been observed under open-circuit conditions and it was found that the location of catalyst precipitation is affected by the fuel permeation through the membrane [22]. Finally, the negative effect of fuel crossover on OCV is particularly significant for direct alcohol fuel cells [23–26]. The current modeling framework can also be extended to explicate these findings.

## 7. Conclusion

We provide a simple model that predicts the effect of fuel permeation on open-circuit voltage in PEM fuel cells. Model predictions are entirely consistent with the experimental observation. To segregate the effect of oxygen versus hydrogen crossover, we find that the crossover current due to oxygen permeation does not significantly affect the anode overpotential and hence has no noticeable effect on the observed OCV. For a pin-hole free membrane, electrical short-circuit current is an order of magnitude smaller than the $H_2$ permeation current. Thus, it is shown that hydrogen crossover entirely accounts for the observed loss of about 0.2 V under open-circuit conditions. The OCV, furthermore, is an important diagnostic tool to determine the physical well-being of the membrane during prolonged operation, and to identify any membrane degradation in the form of membrane thinning or pin-hole formation.

## References

[1] J. Zhang, Y. Tang, C. Song, J. Zhang, H. Wang, J. Power Sources 163 (2006) 532–537.
[2] J.P. Hoare, The Electrochemistry of Oxygen, Interscience Publishers, New York, 1968.
[3] J.O.M. Bockris, S. Srinivasan, Fuel Cells: Their Electrochemistry, McGraw-Hill, New York, 1969.
[4] J. Laraminie, A. Dicks, Fuel Cell Systems Explained, John Wiley, Chichester, England, 2000.
[5] B. Sompalli, B.A. Litteer, W. Gu, H.A. Gasteiger, J. Electrochem. Soc. 154 (2007) B1349–B1357.
[6] S.S. Kocha, J.D. Yang, J.S. Yi, AIChE. J. 52 (2006) 1916–1925.
[7] T. Thampan, S. Malhotra, J. Zhang, R. Datta, Catal. Today 67 (2001) 15–32.
[8] T. Sakai, H. Takenaka, N. Wakabayashi, Y. Kawami, E. Torikai, J. Electrochem. Soc. 132 (1985) 1328–1332.
[9] T. Sakai, H. Takenaka, E. Torikai, J. Electrochem. Soc. 133 (1986) 88–92.
[10] K. Broka, P. Ekdunge, J. Appl. Electrochem. 27 (1997) 117–132.
[11] F. Damay, L.C. Klein, Solid State Ionics 162–163 (2003) 261–267.
[12] R.M. Pashley, M. Rzechowicz, L.R. Pashley, M.J. Francis, J. Phys. Chem. B 109 (2005) 1231–1238.
[13] C. Song, Y. Tang, J.L. Zhang, J. Zhang, H. Wang, J. Shen, S. McDermid, J. Li, P. Kozak, Electrochim. Acta 52 (2007) 2552–2561.
[14] C. Song, J. Zhang, in: J. Zhang (Ed.), PEM Fuel Cell Electrocatalysts and Catalyst Layers, Springer, New York, NY, 2008.
[15] K.C. Neyerlin, W. Gu, J. Jorne, H.A. Gasteiger, J. Electrochem. Soc. 153 (2006) A1955–A1963.
[16] S. Cleghorn, J. Kolde, W. Liu, in: W. Vielstich, A. Lamm, H.A. Gasteiger (Eds.), Handbook of Fuel Cells—Fundamentals, Technology and Applications, John Wiley & Sons, New York, 2003, p. 566.
[17] M. Inaba, T. Kinumoto, M. Kiriake, R. Umebayashi, A. Tasaka, Z. Ogumi, Electrochim. Acta 51 (2006) 5746–5753.
[18] E. Endoh, S. Terazono, H. Widjaja, Y. Takimoto, Electrochem. Solid-State Lett. 7 (2004) A209–A211.
[19] W. Liu, M. Crum, ECS Trans. 3 (2006) 531–540.
[20] H. Tang, S. Peikang, S.P. Jiang, F. Wang, M. Pana, J. Power Sources 170 (2007) 85–92.
[21] C.A. Reiser, L. Bregoli, T.W. Patterson, J.S. Yi, J.D. Yang, M.L. Perry, J.D. Jarvi, Electrochem Solid-State Lett. 8 (2005) A273–A276.
[22] J.-X. Zhang, B.A. Litteer, W. Gu, H. Liu, H.A. Gasteiger, J. Electrochem. Soc. 154 (2007) B1006–B1011.
[23] V.M. Barragan, A. Heinzel, J. Power Sources 104 (2002) 66–72.
[24] K.-M. Yin, J. Power Sources 167 (2007) 420–429.
[25] B.K. Kho, B. Bae, M.A. Scibioh, J. Lee, H.Y. Ha, J. Power Sources 142 (2005) 50–55.
[26] S. Song, W. Zhou, J. Tian, R. Cai, G. Sun, Q. Xin, S. Kontou, P. Tsiakaras, J. Power Sources 145 (2005) 266–271.